J Mater Sci (2011) 46:7822–7829
DOI 10.1007/s10853-011-5763-6

# Study on mechanism of enhanced photocatalytic performance of N-doped $TiO_2$/Ti photoelectrodes by theoretical and experimental methods

**Yanjun Xin · Huiling Liu · Lei Han**

Received: 6 May 2011 / Accepted: 30 June 2011 / Published online: 9 July 2011


**Abstract** Several kinds of N-doped/undoped $TiO_2$ photoelectrodes with different nanostructures have been successfully prepared by anodization method and plasma-based ion implantation (PBII) technique. The morphology and structure of as-prepared photoelectrodes were studied by scanning electron microscopy, X-ray diffraction, and ultra violet/visible light diffuse reflectance spectra. Electronic structure and optical properties were calculated by means of first-principle. Photocatalytic (PC) and photoelectrocatalytic (PEC) performance were measured by the decomposition of terephthalic acid (TA) and Rhodamine B under xenon light illumination. Theoretical calculation results demonstrated that crystal phases have great influence on the electric and optical properties, and N-doped $TiO_2$ photoelectrodes have isolated $N_{2P}$ impurity states nearby the top of the valence band. The optical properties and UV/Vis analysis confirmed that the absorption edge of N–$TiO_2$ emerged red-shift and high photosensitivity. The discrepancy of PC and PEC performance of as-prepared $TiO_2$ photoelectrodes were ascribed to band gap narrowing, $N_{2p}$ impurity states, self-semiconductor coupling effect, and long-range ordered orientation of photogenerated carries originated from applied electric field.

Y. Xin · H. Liu (✉) · L. Han
Department of Environmental Science and Engineering, State Key Laboratory of Urban Water Resources and Environment (SKLUWRE), Harbin Institute of Technology, Huanghe Road 73, Nangang, Harbin 150090, China
e-mail: hlliu2002@163.com; xintom770824@yahoo.com.cn

Y. Xin
School of Resource and Environment, Qingdao Agricultura1 University, Qingdao 266109, China

L. Han
School of Environmental and Chemical Engineering, Dalian Jiaotong University, Dalian 116028, China

## Introduction

In the past three decades, $TiO_2$ photocatalysis has been extensively studied throughout the world for water and wastewater treatment because of its nontoxicity, photochemical stability, and low costs [1–5]. Unfortunately, $TiO_2$ photocatalyst has a band gap of 3.2 eV, and can only be activated under UV radiation ($\lambda < 380$ nm), which occupies only less than 5% of the solar irradiance at the Earth's surface [6]. For the efficient use of sunlight, many methods have been researched, including transition metal and rare earth element doping [7–9], noble deposition [10, 11], semiconductor coupled [12], dye sensitization [13, 14], etc [15, 16]. Since Asahi et al. [6] reported that N-doped $TiO_2$ could extend the photoactive region to visible spectral range, and nitrogen doping becomes a research hotspot in recent years [17–20]. Up to now, various mechanisms have been proposed to account for the visible light activity of N-doped $TiO_2$ [21–23].

In recent years, CASTEP code based on density functional theory (DFT) has been successfully used to study crystal structure, electronic structure, and optical properties [24–28]. So far, many researchers carried out a large number of investigations on $TiO_2$ photocatalyst by first principles based on DFT [29–31], but little researchers focused on the influence of crystal phases. To fundamentally understand such structure–activity relationships of $TiO_2$ photocatalyst, it was important to deep insight into the microstructure of crystal phase and PC and PEC activity of various $TiO_2$ photoelectrodes. Furthermore, to the best of our knowledge, there were little reports on the

systematic investigation about the correlation between the band gap, optical properties, and PC and PEC degradation efficiency of organic pollutants using different crystal $TiO_2$ photoelectrodes from both theoretical and experimental aspects.

In previous research, N–$TiO_2$ photoelectrodes were successfully fabricated by plasma-based ion implantation (PBII) method at low temperature on situ growth of $TiO_2$ photoelectrode from titanium substrate [16]. In this study, the effects of nitrogen doping on the electronic structure and optical properties of single anatase or rutile $TiO_2$ were examined using plane wave pseudopotential and supercell model based on CASTEP software package. The influence of nitrogen doping on the properties of $TiO_2$/Ti photoelectrode was explored by means of theoretical calculation and experimental investigation, including electrode characterization and PC and PEC decomposition rate of organic pollutants.

It could be great significant for practical application of first principles in water treatment and might provide a new method for the mechanism analysis of PC and PEC properties of modified $TiO_2$/Ti photoelectrodes or other photocatalysts.

## Experimental

### Experimental chemicals and materials

Titanium (Ti) foils (purity >99.5%, 0.2-mm thickness) were purchased from Baoji Titanium and Nickel Manufacture Limited Company, China. Other chemicals were obtained as analytical reagent grade and used without further purification. Experimental solutions were prepared with doubly distilled water.

### Sample preparation and characterization

N-doped and undoped $TiO_2$/Ti photoelectrodes were fabricated according to the previous results [16]. Pure photoelectrodes were fabricated in a dual-electrode reaction chamber. Cleaned Ti foil and copper foil of the same size were used as the anode and cathode, respectively. Two electrodes with a distance of 3 cm were submerged into 0.5 mol/L $H_2SO_4$ solution. The current of 500 mA was supplied from the beginning of the oxidation reaction until the voltage reached a series of determined value (120, 160, and 200 V). The total reaction time was 10 min. After the process, samples were immediately rinsed with deionized water and dried in 378 K for 30 min. N-ions were implanted into as-prepared $TiO_2$/Ti photoelectrode by PBII under 573 K and labeled as N-120, N-160, and N-200, respectively, where the numbers represented the determined voltage. Similarly, undoped $TiO_2$/Ti photoelectrodes were labeled as P-120, P-160, and P-200.

Surface morphologies of as-prepared photoelectrodes were studied by scanning electronic microscopy (SEM). Crystal structures were examined using D/max-rB X-ray diffraction (XRD) with CuK$\alpha$ radiation ($\lambda = 1.54050$). Measurements were performed at 0.02° intervals of $2\theta$ over the range of 10°–90°. Diffuse reflectance spectra (DRS) were recorded using Lambda 900 UV/Vis spectrophotometer with a diffuse reflectance accessory.

### PC and PEC activity evaluation

PC and PEC performance of different $TiO_2$/Ti photoelectrodes were evaluated via the yield of $^{\bullet}OH$ radical and the discoloration rate of Rhodamine B (Rh.B) in sample solutions.

The yield of $^{\bullet}OH$ radical was performed by fluorescence technique in terephthalic acid (TA) solution, which readily reacted with $^{\bullet}OH$ radicals to produce fluorescent product, 2-hydroxyterephthalic acid (TAOH) [32]. The concentration of TA was $3 \times 10^{-4}$ M. According to the literature [33], the intensity of fluorescence peak at 426 nm was attributed to TAOH.

Sample solutions were irradiated by 75 W xenon light, which mainly provided wavelength in the range of 380–800 nm. Before photoreaction, the solution was magnetically stirred in dark for 30 min to reach adsorption/desorption equilibrium and then was illuminated with stirring. The intensity of TAOH was measured using fluorescence spectrophotometer (Jasco FP-6500) and the photodiscoloration rate of Rh.B was analyzed using UV/Vis spectrophotometer(UV2500, SHIMADZU).

### Theoretical calculations

All calculations were carried out by CASTEP code, which was based on DFT approach. The exchange and correlation interactions were modeled using the generalized gradient approximation (GGA) [34], together with the Perdew–Burke–Ernzerhof (PBE) [25, 30] exchange–correlation functional and ultrasoft pseudopotentials. The core electrons were replaced by the ultrasoft core potentials, and the valence atomic configurations were $3s^2 3p^6 3d^2 4\ s^2$ for Ti, $2s^2 2p^4$ for O, and $2s^2 2p^3$ for N atom. For the sake of comparison, 48-atom supercells were used to construct $TiO_2$ models for calculation. For N-doped $TiO_2$, one oxygen atom in the supercell was replaced by a nitrogen atom. The fraction of nitrogen atomic content was 2.08%, which was comparable to the fraction of 2.09% of as-prepared N-doped photoelectrodes. The cut-off energy of 340 eV and a $3 \times 3 \times 3$ k-point set centered at point were sufficient to make the total energy converge to within a

tolerance of $10^{-6}$eV/atom. The lattice parameters and the atomic positions were fully optimized until all components of the residual forces were smaller than 0.05 eV/Å.

In the calculations, the cell parameters and atomic coordinates were optimized, so the total energy of the structure was minimized and stable structure for all models could be obtained. For comparing the band gap, electronic structures and optical properties of different $TiO_2$ photoelectrodes conveniently, the same optimization and calculation conditions were used. In order to obtain comparable results with the experiments, unpolarized polycrystalline models and "scissors operators" [35], which were introduced to shift all the conduction levels to meet with the measured value of the band gap, were used. A rigid scissor operator correction of 1.0 eV was applied for anatase $TiO_2$ (P-120 and N-120) photoelectrodes and rutile $TiO_2$ (P-200 and N-200) to keep consistence with the experimental band gap (3.2 eV for anatase $TiO_2$ and 3.0 eV for rutile $TiO_2$).

## Results and discussions

### Structure and morphology

It was well known that crystal structure significantly affected PC activity of $TiO_2$ photoelectrodes. The amorphous $TiO_2$ showed little PC activity due to crystal defect state, i.e., the unbonded oxygen, which could become the recombination centre of photoelectron and hole. So, in the manuscript the amorphous $TiO_2$ photoelectrode was not considered. XRD of N-doped and undoped $TiO_2$ photoelectrodes prepared in different voltage were shown in Fig. 1 (XRD patterns of P-120 and P-200 photoelectrodes were not shown for similar with that of N-120 and N-200 photoelectrodes). The results in Fig. 1 displayed that the crystal structures of N-120 photoelectrode were mainly composed of anatase $TiO_2$ and that of N-200 photoelectrode were rutile $TiO_2$. However, both N-160 and P-160 photoelectrodes were composed of mixed anatase and rutile $TiO_2$. For N-doped $TiO_2$ photoelectrodes, none of nitrogen compound peak was detected by XRD, but XRF results revealed the accurate percent of nitrogen content was 2.09%. The nitrogen content was high enough to be detected by XRD if any nitrogen compounds formed. Since no other crystalline peaks were detected, the nitrogen atoms might be introduced into $TiO_2$ crystal lattice, which has been verified by our workgroup [16].

According to the indexation of peaks, the fraction of rutile in N-160 photoelectrodes was higher than that in P-160 photoelectrodes. For the composite photoelectrodes, the fractions of anatase and rutile phase were estimated according to the literature [36]. The calculation results revealed that the ratios of anatase and rutile crystal in N-160 and P-160 photoelectrodes were 41:59 and 55: 45, respectively.

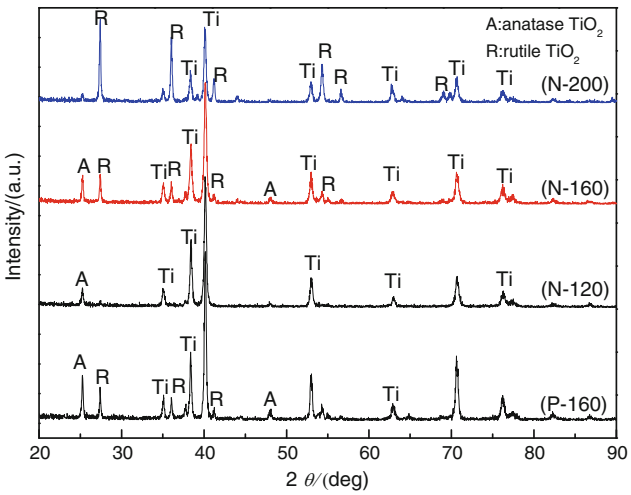


**Fig. 1** XRD patterns of N-doped and pure $TiO_2$ photoelectrodes

The morphologies of different $TiO_2$ photoelectrodes were examined by SEM and showed in Fig. 2. It could be observed that P-160 $TiO_2$ photoelectrode showed gray color, while N-doped $TiO_2$ photoelectrodes were light yellow. Average apertures of N-120, N-160, and N-200 photoelectrodes were ~90, ~200, and ~500 nm, which were the same with P-120, P-160, and P-200 photoelectrodes (the images of P-120 and P-200 photoelectrodes were not shown). All images clearly demonstrated that the samples' surfaces were rough and porous, and the average apertures of them increased with voltage.

### Band structure

Based on XRD results, N-120 and P-120 were used to stand for anatase N-doped and undoped $TiO_2$ models, while N-200 and P-200 represented rutile N-doped and pure $TiO_2$ models, respectively. Band structures of N-120, P-120, N-200, and P-200 photoelectrodes were calculated to analyze the electronic properties. The patterns of band structures were plotted in Fig. 3.

The results in Fig. 3 showed that P-200 photoelectrode has a direct gap at G point and P-120 photoelectrode has an indirect one between G and F, which were in accordance with previously reported results [25, 37], while both N-120 and N-200 photoelectrodes have indirect one between G and F. For both N-120 and N-200 photoelectrodes, the energy levels were split for the decreasing of crystal symmetry caused by ***nitrogen doping, and an impurity energy level located just above the top of valence band (VB), which formed a shallow acceptor. Another important feature was that Fermi level crossed the bottom of impurity energy levels, so it was not fully filled with electrons at

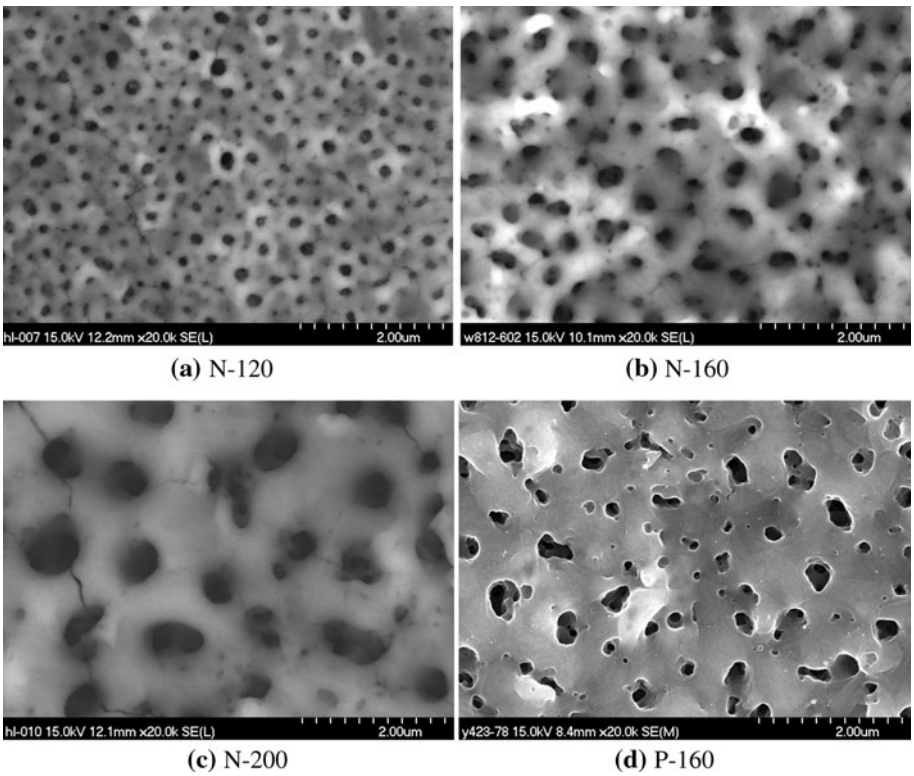


**Fig. 2** SEM of N-doped and pure $TiO_2$ photoelectrodes prepared in different voltage. **a** N-120; **b** N-160; **c** N-200; **d** P-160

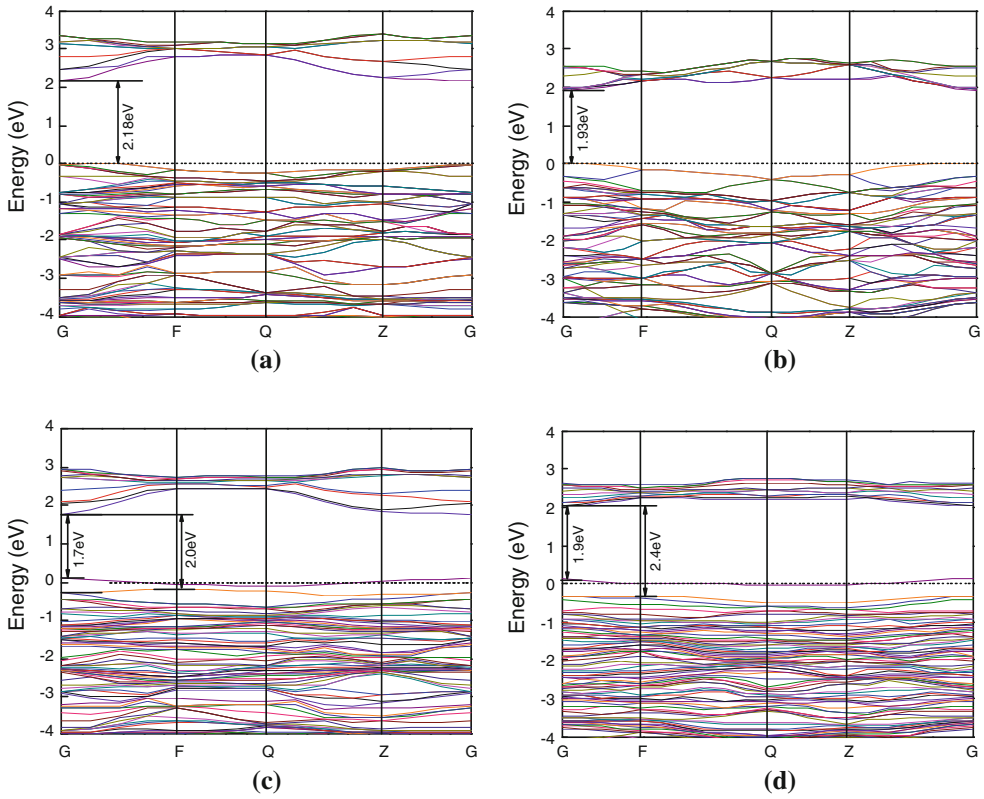


**Fig. 3** Band structure of N-doped and pure $TiO_2$ photoelectrodes. **a** P-120; **b** P-200; **c** N-120; **d** N-200

ground state. For N-120 and P-120 photoelectrodes, the calculated results showed the bottom of conduction band (CB) declined and the band gap changed from 2.18 to 2.0 eV, regardless of the $N_{2P}$ impurity energy levels in the band gap. If the impurity energy level was taken into account, the band gap of N-120 photoelectrode was largely

narrowed to 1.7 eV. However, for N-200 photoelectrodes, the calculated results showed the top of VB declined and the band gap was a littlie narrower if the $N_{2P}$ impurity energy level was taken into account. The results showed that the electronic structure of anatase $TiO_2$ was more susceptible to the influence of nitrogen than that of rutile $TiO_2$. Furthermore, the shallow acceptor acted as a trap for photoexcited carriers, and the electron–hole pairs would separate more easily. At the same time, the narrower band gap could make the fundamental absorption edges red-shift toward visible light region. Thus, N-120 and N-200 photoelectrodes might show better photocatalytic performance. The results were consistent with the previous study and provided a good explanation for the red-shift observed in recent experiments [38, 39].

## Optical properties

On the basis of CASTEP code, optical absorption spectra of P-120, P-200, N-120, and N-200 photoelectrodes obtained from theoretical calculations were plotted in Fig. 4, and UV/Vis DRS spectra of P-160 and N-160 photoelectrodes were plotted in Fig. 5.

The calculated results in Fig. 4 showed that N-120 and N-200 photoelectrodes have stronger photoresponse than P-120 and P-200 photoelectrodes in the visible region ($\lambda > 400$ nm). The results demonstrated that nitrogen doping could result in red-shift of the absorption spectra and were in accordance with band structure properties (Fig. 3). P-200 photoelectrodes presented a little red-shift and higher photoresponse comparing with P-120 photoelectrodes, which might be ascribed to the narrower band gap of rutile $TiO_2$ than that of anatase $TiO_2$. N-200

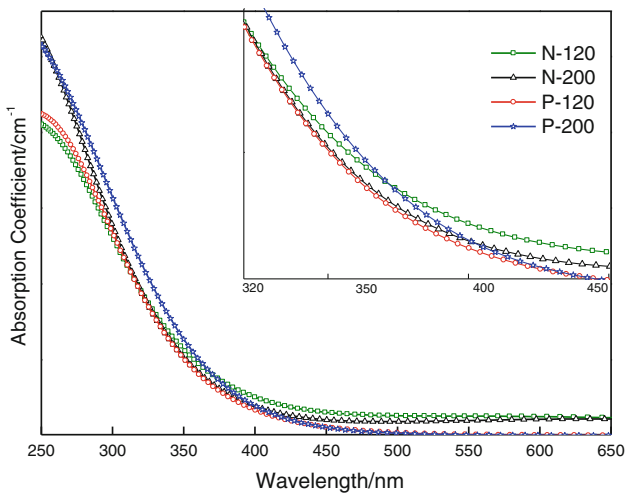


**Fig. 4** Calculated optical absorption curves of P-120, P-200, N-120, and N-200 photoelectrodes

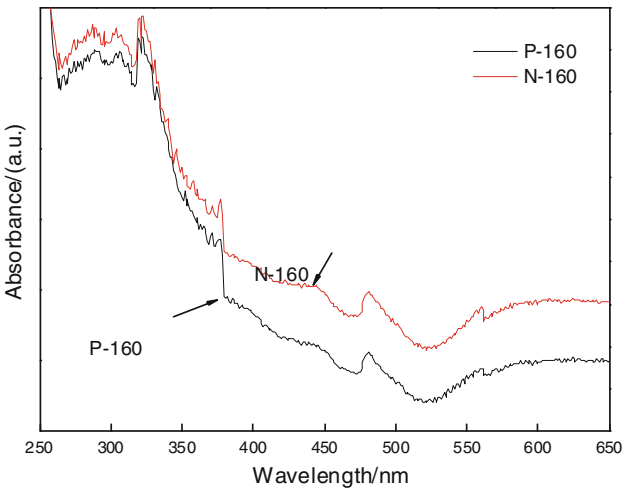


**Fig. 5** UV/Vis DRS spectra of P-160 and N-160 photoelectrodes

photoelectrodes presented stronger photoresponse than N-120 photoelectrodes in ultraviolet region, but it was reverse in visible region, which might be ascribed to the different crystal structures of N–$TiO_2$ photoelectrodes.

The results in Fig. 5 showed that in whole light region the absorption intensity of N-160 photoelectrode increased significantly comparing with that of P-160 photoelectrode, which revealed that the N-160 photoelectrodes were more sensitive to light. In the meantime, a shift of the absorption threshold toward the visible light region was also observed for N-160 photoelectrodes. UV/Vis results further demonstrated that the nitrogen incorporated into $TiO_2$ lattice would extend absorption threshold toward the visible light region, which could promote PC activity of $TiO_2$ photoelectrodes. In conclusions, the calculation results of optical properties and UV/Vis/DRS spectra demonstrated that crystal structure and nitrogen doping would influence photosensitivity of $TiO_2$ photoelectrodes; in particular, nitrogen doping could improve greatly the visible light response of $TiO_2$ photoelectrodes.

## PC and PEC activity

Based on the literatures [32, 40], when the concentration of TA was less than $10^{-3}$ M at room temperature, the hydroxylation reaction of TA proceeded mainly by $^{\bullet}OH$ radicals and the peak intensity of TAOH was known to be proportional to the yield of $^{\bullet}OH$ radicals. Thus, stronger fluorescence intensity meant higher yield of $^{\bullet}OH$ radical and could achieve higher photocatalytic performance. The results in Fig. 6 showed the characteristic peak of terephthalic acid (TPA) solution declined with the trend of N-160-PEC > P-160-PEC > N-160 > N-200 > P-160 > N-120 ≈ P-200 > P-120, which was similar with the discoloration rates of Rh.B presented in Fig. 7.

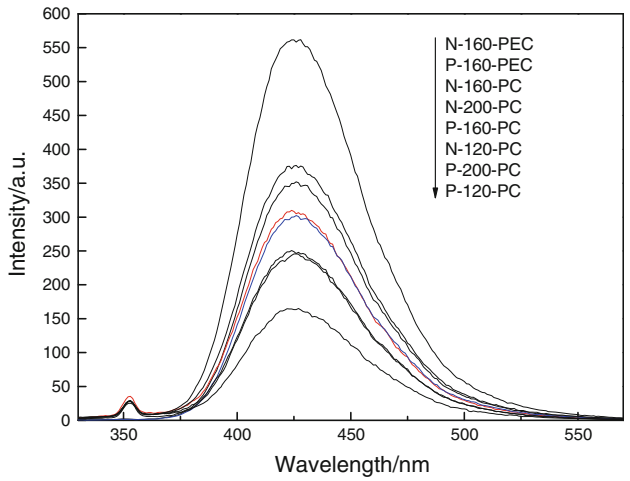


**Fig. 6** Fluorescence intensity of N-doped and pure $TiO_2$/Ti photoelectrodes

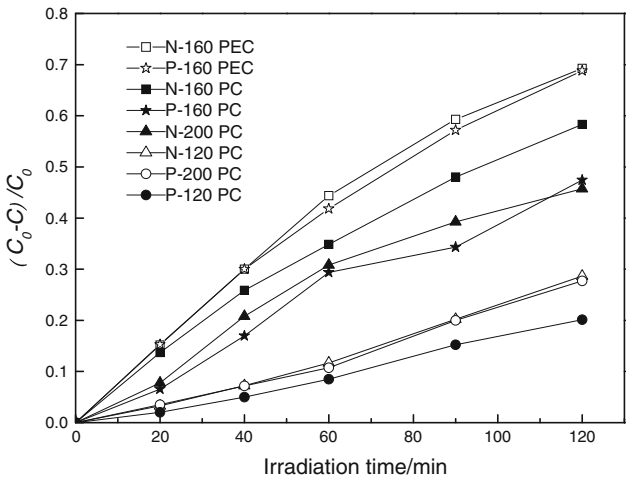


**Fig. 7** Rh.B discoloration rate of N-doped and pure $TiO_2$/Ti photoelectrodes

The results showed that the peak value at 426 nm of N-160 photoelectrodes was 1.5 times to that of P-160 photoelectrodes with the applied potential at 1.0 V, while the ratio was only 1.2 times without bias potential. The peak value of N-160 photoelectrode at 1.0 V bias potential was 1.6 times than without bias potential, while the ratio of P-160 photoelectrodes was only 1.25 times. The results indicated that the bias potential promoted the separation efficiency of photogenerated charges of N-160 and P-160 photoelectrodes, in particular, the separation efficiency of the photogenerated electron–hole pairs originated from N-160 photoelectrodes. The higher separation rate predicted the higher PC and PEC activity, which were verified by the photodiscoloration tests of Rh.B.

The results in Fig. 7 showed that the photodiscoloration rates of Rh.B as a function of time were following the same trend with the yield of $^{\bullet}OH$ radicals (Fig. 6). PC activities of P-200 photoelectrodes were higher than that of P-120 photoelectrodes for rutile $TiO_2$ have narrower band gap and stronger photosensitivity than anatase $TiO_2$. The high PC activities of P-160 photoelectrodes were ascribed to the mixed crystal effect, which would promote the separation of photogenerated electron–hole pairs. $N_{2P}$ impurity states could cause red-shift and increase the photoresponse of $TiO_2$ photoelectrodes, which would increase PC activity of N-doped photoelectrodes. Besides the former factors, the highest PEC activities of N-160 and P-160 photoelectrodes were also owing to the effect of 1.0 V assistant potentials. However, there was an interesting phenomenon that photodiscoloration rates of Rh.B by N-160 and P-160 photoelectrodes at 1.0 V bias potentials were very close, which was different from the yield of $^{\bullet}OH$ radicals (Fig. 6). The difference might be ascribed to the change in reaction determining step, which was transformed from the hydroxyl radical control in the initial to the mass transfer control later. These have been observed experimentally and would be discussed at later. In a word, the variation of removal rates of Rh.B were accordance with the yield of $^{\bullet}OH$ radicals, which also verified that the bias potential, mixed crystal, and nitrogen doping could promote PC activity of $TiO_2$/Ti photoelectrodes.

Taking into account the former results, the possible transmission process of photo-generated charges and degradation pathway of Rh.B could be summarized in Scheme 1. $N_{2P}$ impurity states reduced band gap of N-120, N-160, and N-200 photoelectrodes (Scheme 1a and b) and increased the available light; therefore, the PC activity of N-doped $TiO_2$ photoelectrodes would be promoted. Mixed crystal structure would facilitate the separation of photogenerated electrons and holes due to the self-semiconductor coupling effect (Scheme 1c), which was responsible for the higher PC performance of P-160 photoelectrodes. N-160 photoelectrode has the highest photodiscoloration rate of Rh.B in all $TiO_2$ photoelectrodes due to the cooperation of $N_{2p}$ impurity level and mixed crystal structure (Scheme 1d). When bias potentials was applied, the moving direction of photogenerated electrons and holes would change from random to orientation under the effect of electric field (Scheme 1b and c), so the recombination opportunities reduced greatly. In conclusions, the integration effect of the former reasons were responsible for the discrepancy of PC and PEC performance of N-120, N-160, N-200, P-200, P-160, and P-120 photoelectrodes.

## Conclusions

In this study, N-200, N-160, N-120, P-200, P-160, and P-120 $TiO_2$ photoelectrodes have been prepared by anodization and PBII technique. The first-principle calculation

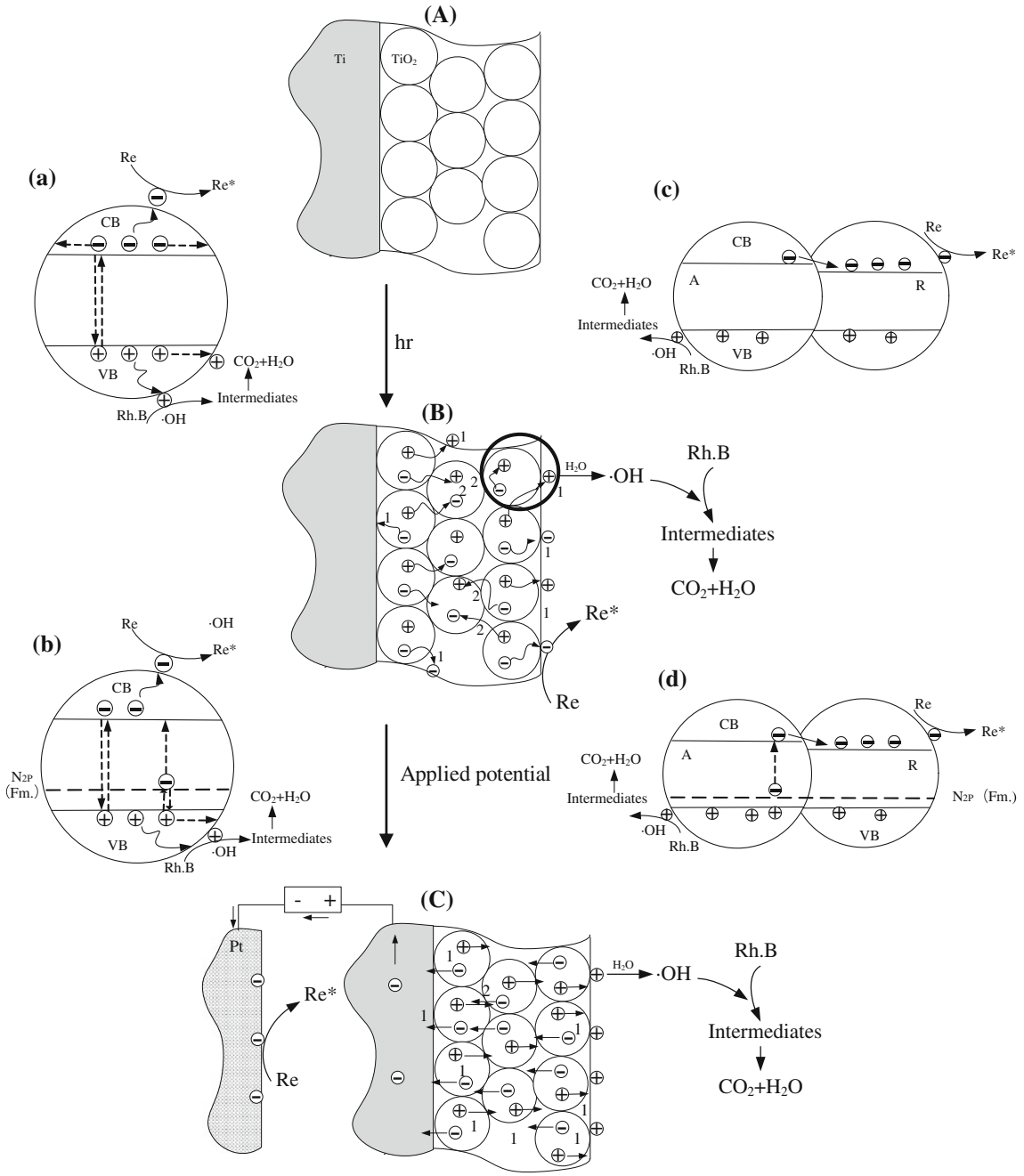


**Scheme 1** Schematic illustration of photophysical chemistry process in different $TiO_2$ photoelectrodes. (*A*) Microstructure of $TiO_2$ photoelectrodes; (*B*) movement of photoelectrons and holes without bias potentials; (*C*) movement of photoelectrons and holes at applied bias potentials; **a**, **b**, and **c** were the transmission of photogenerated electrons and holes of local enlargement of (*B*) (*black open circle*); **a** carriers movement in P-120 and P-200 photoelectrodes (undoped single crystal); **b** carriers movement in N-100 and N-200 photoelectrodes (N-doped single crystal); **c** carriers movement in P-160 photoelectrodes (undoped mixed crystal); **d** carriers movement in N-160 $TiO_2$ photoelectrode (N-doped mixed crystal); (*1*) Transmission process of photoelectrons and holes; (*2*) Recombination process of photoelectrons and holes. *Arrow* represents move direction of photo-carriers

results showed that crystal structure and nitrogen doping could significantly affect the band gap and optical properties of $TiO_2$. Anatase or rutile $TiO_2$ with substitution nitrogen has isolated impurity states nearby the top of VB, which make photoexcited electron–hole pairs separate easily. The mixed anatase/rutile self-semiconductor coupling effect of N-160 and P-160 photoelectrodes also promoted further the separation efficiency of photogenerated electrons and holes. Assistant potentials could make the moving direction of photogenerated electrons and holes

change from random to orientation, thus reduced the recombination of photogenerated charges. All the integration effects including crystal structure, $N_{2p}$ impurity states, self-semiconductor coupling effect, and long-range orientation of photogenerated carries were responsible for the trend of PC and PEC activities of N-160-PEC > P-160-PEC > N-160 > N-200 > P-160 > N-120 > P-200 > P-120.

**Acknowledgements** This study was supported by National Natural Science Foundation of China (No. 50978066), National Creative Research Groups of National Natural Science Foundation of China (No. 50821002) and State Key Laboratory of Urban Water Resources and Environment (No. 2010DX03).

## References

1. Vinodgopal K, Hotchandani S, Kamat PV (1993) Phys Chem 97:9040
2. Alfano OM, Bahnemann D, Cassano AE, Dillert R, Goslich R (2000) Catal Today 58:199
3. Candal RJ, Zeltner WA, Anderson MA (2000) Environ Sci Technol 34:3443
4. Calvo ME, Candal RJ, Bilmes SA (2001) Environ Sci Technol 35:4132
5. Li XZ, Liu HS (2005) Environ Sci Technol 39:4614
6. Asahi R, Morikawa T, Ohwaki T, Aoki K, Taga Y (2001) Science 293:269
7. Li FB, Li XZ, Hou MF, Cheah KW, Choy WCH (2005) Appl Catal A Gen 285:181
8. Peng HS, Huang SH, You FT, Chang JJ, Lu SZ, Cao L (2005) J Phys Chem B 109:5774
9. Wu JCS, Chen CH (2004) J Photochem Photobiol A Chem 163:509
10. Yu JG, Xiong JF, Cheng B, Liu SW (2005) Appl Catal B Environ 60:211
11. Seery MK, George R, Floris P, Pillai SC (2007) J Photochem Photobiol A Chem 189:258
12. Kanjwal MA, Barakat NAM, Sheikh FA, Kim HY (2010) J Mater Sci 45:1272. doi:10.1007/s10853-009-4078-3
13. Macak JM, Tsuchiya H, Ghicov A, Schmuki P (2005) Electrochem Commun 7:1133
14. Alex S, Santhosh U, Das S (2005) J Photochem Photobiol A Chem 172:63
15. Xie YB, Li XZ (2006) J Hazard Mater 138:526
16. Han L, Xin YJ, Liu HL, Ma XX, Tang GZ (2010) J Hazard Mater 175:524
17. Li DZ, Chen ZX, Chen YL, Li WJ, Huang HJ, He YH, Fu XZ (2008) Environ Sci Technol 42:2130
18. Tessier F, Zollfrank C, Travitzky N, Windsheimer H, Zollfrank C, Conanec OM, Rocherulle J, Greil P (2009) J Mater Sci 44:6110. doi:10.1007/s10853-009-3845-5
19. Rengifo-Herrera JA, Pierzchala K, Sienkiewicz A, Forro L, Kiwi J, Pulgarin C (2009) Appl Catal B Environ 88:398
20. Kobayakawa K, Murakami Y, Sato Y (2005) J Photochem Photobiol A Chem 170:177
21. Irie H, Watanabe Y, Hashimoto K (2003) J Phys Chem B 107:5483
22. Valentin CD, Pacchioni G, Selloni A, Livraghi S, Giamello E (2005) J Phys Chem B 109:11414
23. Livraghi S, Paganini MC, Giamello E, Selloni A, Valentin CD, Pacchioni G (2006) J Am Chem Soc 128:15666
24. Deskins NA, Dupuis M (2007) Phys Rev B 75:195212
25. Labat F, Baranek P, Domain C, Minot C, Adamo C (2007) J Chem Phys 126:154703
26. Yang KS, Dai Y, Huang BB, Feng YP (2010) Phys Rev B 81:033202
27. Yang KS, Dai Y, Huang BB, Whangbo MH (2009) J Phys Chem C 113:2624
28. Quenneville J, Ben-Nun M, Martinez TJ (2001) J Photochem Photobiol A Chem 144:229
29. Tao JG, Guan LX, Pan JS, Huan CHA, Wang L, Kuo JL, Zhang Z, Chai JW, Wang SJ (2009) Appl Phys Lett 95:062505
30. Finazzi E, Valentin CD, Selloni A, Pacchioni G (2007) J Phys Chem C 111:9275
31. Tsetseris L (2010) Phys Rev B 81:165205
32. Ishibashi K, Fujishima A, Watanabe T, Hashimoto K (2000) Electrochem Commun 2:207
33. Xiao Q, Si ZC, Zhang J, Xiao C, Tan XK (2008) J Hazard Mater 150:62
34. Perdew JP, Burke K, Ernzerhof M (1996) Phys Rev Lett 77:3865
35. Godby RW, Schluter M, Sham LJ (1988) Phys Rev B 37:10159
36. Song XM, Wu JM, Tang MZ, Qi B, Yan M (2008) J Phys Chem C 112:19484
37. Long MC, Cai WM, Wang ZP, Liu GZ (2006) Chem Phys Lett 420:71
38. Lindgren T, Mwabora JM, Avendano E, Jonsson J (2003) J Phys Chem B 107:5709
39. Batzill M, Morales EH, Diebold U (2006) Phys Rev Lett 96:026103
40. Hirakawa T, Yawata K, Nosaka Y (2007) Appl Catal A Gen 325:105